Copper(II) solvatochromic complexes [Cu(acac)(N^N)(ligand)]BPh_4 with various axial ligands. Correlation between coordination geometries and d-d transition energies (acac = acetylacetonato, N^N = 1,10-phenanthoroline, 2,2′-bipyridyl)

Ryo Horikoshi [a,*], Yusuke Funasako [b], Takeshi Yajima [a], Tomoyuki Mochida [b], Yoji Kobayashi [a], Hiroshi Kageyama [a]

[a] *Department of Energy and Hydrocarbon Chemistry, Graduate School of Engineering, Kyoto University, Nishikyo-ku, Kyoto 615-8510, Japan.*

[b] *Department of Chemistry, Graduate School of Science, Kobe University, Rokkodai, Nada, Kobe Hyogo 657-8501, Japan.*

* Corresponding author. FAX: +81 75 383 2510

E-mail address: horikoshi.ryo.3u@kyoto-u.ac.jp

Keywords: Structure elucidation; Solvatochromism, Copper complex; O ligands; N ligands

ABSTRACT

A series of copper(II) solvatochromic complexes [Cu(acac)(N^N)(ligand)]BPh_4 (acac = acetylacetonato; N^N = 1,10-phenanthoroline (**1**), 2,2′-bipyridyl (**2**); ligand = HMPA, pyridine, DMSO, DMF, MeOH, acetone, and MeCN) have been synthesized and their coordination geometries were crystallographically investigated. The solvent-coordinated cations, adopting a five-coordinate square-pyramidal structure, formed head-to-tail dimers via π···π interactions. Solid-state absorption studies revealed that their d-d transition energies are correlated with the donor number of the axial ligands. A linear correlation was found between the d-d transition

energies and the Cu−O (axial ligands) distances in the solid-state, revealing the role of the coordination environment on the d-d transition energies in the copper(II) solvatochromic complexes.

1. Introduction

Chromotropism of coordination compounds, or color change due to external stimuli, is an interesting phenomenon and is generally ascribed to transformation of coordination geometry around the metal center [1–5]. In particular, the solvatochromism of metal complexes have attracted special attention because of their potential application for color indicators and optical sensors [1–3,6]. To date, many copper(II) solvatochromic complexes with mixed ligands have been reported, in which chelate ligands of *β*-diketonato and ethylenediamine derivatives are often used [1–16]. Solutions of these complexes show color changes from green via blue to violet, depending on the solvent. The color change originates from the shift of the d-d absorption bands of the copper(II) center by coordination of the solvent molecules. The absorption energies are known to correlate with the donor number (DN) of the coordinated solvents [1–16]. In the solvent-coordinated species, the coordination geometries around the metal center should be a crucial factor that determines the d-d absorption energies. However, a systematic study of the correlation between the coordination environments and the d-d absorption bands of metal(II) solvatochromic complexes has not been reported, whereas there have been a few structural reports on solvent coordinated copper(II) solvatochromic complexes [8,12].

In this context, to investigate solvent dependence of the coordination environment and its consequence on the solvatochromism, we have designed square planar complexes [Cu(acac)(N^N)]BPh_4 {acac = acetylacetonato, N^N = 1,10-phenanthoroline (phen) (**1**) or 2,2′-bipyridyl (bpy) (**2**)} (Fig. 1), expecting that the use of planar ligands leads to π···π interactions and which consequently provides crystalline materials suitable for crystallography. In fact, copper(II) complexes with *β*-diketonato and aromatic *N*-donor ligands have been used as building blocks for supramolecular architectures [17–21]. Most of such complexes are anion-coordinated neutral species, and have not been investigated from chromotropic aspects. We expected that the use of a bulky and non-coordinating counter anion, BPh_4^-, provides space for solvent coordination

to the metal centre in the crystalline state, which enables direct comparison of the chromic properties in solution and in the solid state. Here we report the preparation, crystal structures, and absorption spectra of unsolvated **1**, **2**, and their solvated states with a wide range of DN, from HMPA (168 $kJmol^{-1}$) to MeCN (59 $kJmol^{-1}$). A correlation was found between the coordination environments, solid state d-d transition energies, and DN of the axial ligands (i.e. solvent). To our knowledge, this is the first study elucidating the structure-property relationship of solvatochromic copper(II) complexes.

2. Results and Discussion

2.1. Synthesis

1 and **2** were prepared by the reaction of $Cu(NO_3)_2{\cdot}3H_2O$ with *N*-chelate ligands (N^N) and acac in the presence of a base in EtOH, followed by anion exchange using $NaBPh_4$. Recrystallization of **1** and **2** from polar solvent with relatively high donor number (DN) provided green or blue crystals of solvent-coordinated complexes, **1**(HMPA), **1**(Py), **1**(DMSO), **1**(DMF), **1**(acetone), **1**(MeCN)·MeCN, **2**(Py), **2**(DMSO), **2**(DMF)·DMF, and **2**(MeOH). Recrystallization from solvents with lower DN (PhCN and $MeNO_2$) afforded violet crystals of **1**, **2**, and **1**·$MeNO_2$, having no axial ligands. **1**·$MeNO_2$ was a nitromethane solvate. This tendency demonstrates the correlation between the DN of solvent molecules and their coordinating abilities. In the IR spectra of the solvent-coordinated complexes, characteristic peaks of the solvent molecules were observed.

2.2. d-d Transition energies in the solid state

Solid state UV-Vis absorption spectra of **1** and its solvated complexes are shown in Fig. 2. The broad absorption bands are assigned to the d-d transitions of the copper(II) ion, and the absorption maxima (ν_{max}) varied depending on the axial ligands (Table 1). A linear correlation was found between the ν_{max} and the DN of the ligands, as shown in Fig. 3. Even the unsolvated samples follow

the same linear trend. ν_{max} of **1**(Py) and **2**(Py) were slightly different from those expected from the DN of pyridine. The d-d transition energies of **1** and its solvated complexes were slightly lower than those of **2** and its solvated complexes. As will be shown in the solvatochromism section, **1** and **2** exhibit distinctive solvatochromism in various solvents, and the d-d transition energies in solutions are comparable to those in the solid complexes with the corresponding solvent. However, the color differences of the crystalline materials were less distinguishable by naked eye because they are bulk samples (Color pictures in Fig. S1, supplementary material).

2.3. Coordination geometries of solvent coordinated complexes

Structures of the solvated cations (L = HMPA, Py, DMSO, DMF, acetone, MeCN, and MeOH) determined by X-ray crystallography are depicted in Figs. 4 and 5. The coordination environments around the copper(II) center in these complexes are five-coordinate square pyramidal [22], in which the equatorial sites are occupied by the acac and N^N ligands. For bond distances around the copper(II) center in the complexes, a tendency was observed where the shorter axial Cu−O or Cu−N bonds result in the longer equatorial ones. Comparison of the complexes with O-donor solvents, **1**(HMPA), **1**(DMSO), **1**(DMF), **1**(acetone), **2**(DMSO), **2**(DMF)·DMF, and **2**(MeOH), demonstrates that the axial Cu−O distance (2.172–2.349 Å) depends on the solvent: solvents with larger DN lead to shorter axial Cu−O distances (Fig. 6a). This is the origin of the correlation between the d-d absorption energy and the DN of the axial ligand in the solvated complexes, as shown above. Furthermore, a distinct linear correlation was observed between the axial Cu−O distances and the d-d absorption energies (Fig. 6b). The copper(II) ions are displaced from the equatorial plane toward the axial ligand by 0.104–0.192 Å, which are also linearly correlated with the d-d absorption energies with relatively high correlation coefficients (Fig. 6c).

In the crystals, the cations form head-to-tail dimers via π···π interactions. Similar dimeric molecular arrangements are observed in [{Cu(acac)(phen)}$_2${Au(CN)$_2$}]ClO$_4$ [17], [{Cu(acac)(phen)}$_2${μ-1,3-bis(4-pyridyl)propane}](ClO$_4$)$_2$·6H$_2$O [18], [Cu(acac)(phen)(NCS)] [19],

[Cu(acac)(phen)(NO_3)]·H_2O [20], and [Cu(acac)(phen)(ClO_4)]·0.5MeCN [21], which are anion-coordinated complexes or coordination polymers. The Cu(acac)(N^N) planes in the dimer are parallel and separated by about 3.4–3.6 Å. The interdimer Cu···Cu distances ranges from 3.656 to 6.365 Å, associated with the difference in the degree of overlap between the cations [17–21].

In **1**(HMPA), two of the three $N(CH_3)_2$ moieties were disordered over two sites in a 0.52:0.48 ratio. The planes of acac and phen in the complex are twisted by 11.48° with respect to one another, which is comparable to those found in related complexes with a bulky counter anion, such as [{Cu(acac)(Me_2bpy)(NCS)}$_2$$HgX_2$] of 8.83° (X = SCN) and 31.04° (X = Cl) [19]. However, the Cu(acac)(N^N) moieties of the other complexes in this work are almost flat. According to the Cambridge Structural Database (CSD), structurally characterized copper(II)-HMPA complexes are rare [23,24].

Although the coordination environments around the metal center in **1**(Py) and **2**(Py) are similar to each other, the orientation of the pyridine rings are different. The torsion angles of N(1)−Cu−N(3)−C in **1**(Py) and **2**(Py) are 48.04° and 7.96°, respectively. A similar difference is observed in a coordination polymer complex [{Cu_2(C_6H_5COO)$_4$}$_2$(4DPDS)$_2$]$_n$ [25].

1(DMSO), **2**(DMSO), and **1**(acetone) were isostructural. The axial ligand in **1**(DMSO) was disordered over two sites in a 0.57:0.43 ratio even at 100 K, whereas those in **2**(DMSO) and **1**(acetone) were ordered. The axial Cu−O distances in **1**(DMSO) and **2**(DMSO) are 2.238(16) Å and 2.238(2) Å, respectively. They are comparable to that found in [{Cu(bpy)(DMSO)}$_2$(μ-1,4-di-(3′-acac)benzene)](ClO_4)$_2$ of 2.235 Å [26]. The axial Cu−O distance of 2.349(1) Å in **1**(acetone) is shorter than that in [Cu(tropolone)(tetramethylethylenediamine)(acetone)]BPh_4 of 2.502 Å [27], and this is presumably ascribed to the use of less steric ligand.

1(MeCN)·MeCN and **2**(DMF)·DMF contained not only coordinated solvent but also non-coordinated solvent. The non-coordinated DMF in **2**(DMF)·DMF could not be precisely located owing to extensive disorder even at 100 K. The coordinated DMF molecule in **1**(DMF) is

oriented almost perpendicular to the cation plane, with the dihedral angle between the mean DMF plane and the equatorial plane of the cation is 81.4°. On the other hand, the coordinated DMF in **2**(DMF)·DMF is tilted with respect to the equatorial plane by 41.1°. The axial Cu−O distances in **1**(DMF) and **2**(DMF)·DMF are 2.264(1) Å and 2.244(2) Å, respectively. In **1**(MeCN)·MeCN, the axial Cu−N distance of 2.399 Å and the Cu−N≡C angle of 151° are similar to those observed in $[Cu_4(Schiff\text{-}base)_2(MeCN)_4](PF_6)_4$ (2.332 Å and 148°) [28] and $[Cu_2(\mu\text{-}ox)(di\text{-}2\text{-}pyridiylamine)_2(MeCN)_2](ClO_4)_2$ (2.322 Å and 157°) [29]. In **2**(MeOH), the axial Cu−O distance of 2.317(2) Å and Cu−O(axial)−C angle of 119° are typical values for methanol coordinated copper(II) complexes [30–32].

2.4. Crystal structures of complexes without axial ligands

1 and **2** were isostructural, and the local structures of **1** and **1**·$MeNO_2$ were similar with each other. The copper(II) centers in these complexes adopt four-coordinated square planar coordination geometry. The bond lengths and angles around the metal center are almost identical to those in $[Cu(acac)(Me_2bpy)]ClO_4$ [19]. The [Cu(acac)(phen)] cations form a centrosymmetric dimer in a head-to-tail arrangement similar to the case of the solvated complexes. The dimer structures of **1** and crystal packing of **1**·$MeNO_2$ are illustrated in Figs. 7(a) and (b), respectively. Within the dimer, the interplane distances between the cations are about 3.3–3.6 Å, which are acceptable values for π···π interactions [33]. The Cu···Cu distances within the dimers in **1**, **2**, and **1**·$MeNO_2$ are 3.56 Å, 3.57 Å, and 5.73 Å, respectively. In the crystals, the dimers are segregated by the BPh_4^- anions. In **1**·$MeNO_2$, the nitromethane molecules are located between the dimeric cations and the anions.

2.5. TG Analysis

The weight loss temperatures and ratios determined by thermogravimetric (TG) analyses are summarized in Table 2. The thermograms of unsolvated **1** and **2** exhibited weight losses at around 135−150°C due to decomposition. The complexes coordinated by solvents with high boiling point

exhibited no clear loss of coordination solvent, showing weight loss due to decomposition at around 135−150 °C. The complexes coordinated by axial ligands with relatively low boiling point mostly showed a corresponding weight loss, after which weight loss by decomposition was observed at around 135−150 °C. Among them, **2**(DMF)·DMF showed stepwise loss of incorporated and coordinated DMF molecules. **1**(MeCN)·MeCN, however, showed gradual weight loss, and loss of the coordinated and incorporated acetonitrile molecules were not distinguished. This is probably ascribed to the weakly coordinated acetonitrile.

2.6. Solvatochromism

1 and **2** exhibited distinctive solvatochromism. Colors of solutions changed from green via blue to violet with decreasing the solvent DN, as generally observed for [Cu(*β*-diketonato)(ethylenediamine)]X [1–3,16]. The d-d absorption energies (ν_{max}) of **1** and **2** in various organic solvents at a concentration of 2 mM (Table 3) were linearly correlated with the DN of the used solvents, as shown in Fig. 8. Regardless of the solvents, ν_{max} of **1** was lower than that of **2**. For both the compounds, ν_{max} in acetone was slightly lower than expected from DN of solvent, while that in methanol was slightly higher. Similar phenomena have been observed in a related complex, [Cu(Cl-acac)(diamine)]ClO_4 [9].

The d-d transition energies for **1** and **2** in solvents at a concentration of 2 mM were red-shifted by 200−1400 cm^{-1} relative to those observed for the corresponding solvent-coordinated complexes in the solid-state. The red-shift tends to increase with increasing the d-d absorption energies. ν_{max} in solutions were concentration-dependent, shifting to lower energies with decreasing the concentration. When the relative intensities the peak at around 33000 cm^{-1}, including the π-π* transitions of the acac moiety [20,21] and the lower frequency shoulder of the N^N ligands, and the d-d transitions are compared, the intensity of the latter band is about 10 times weaker in solutions than in the solid-state. This is in accordance with the Laporte rule, suggesting that the solvated complexes adopt an octahedral geometry in solutions, as often illustrated in literature [1–4].

Consistently, DFT calculations revealed that the octahedrally coordinated complex is more stable than the square pyramidal complex as a gaseous free complex. In the solid state, however, five-coordinate structures were found. Our calculations revealed that, when two water molecules were placed above and below the completely unsolvated cation of **1**, both molecules coordinate to the axial positions of the copper(II) center, although one of them is coordinated rather weakly. The presence of a large amount of solvent molecules in solution enables the cation to adopt octahedral geometry. In contrast, when the concentration of the complex becomes high during recrystallization, the cation forms a π-stacked dimer structure involving the square pyramidal units, due to dipole-dipole interactions. This energy gain by forming the dimer structure probably overcomes that given by coordination of an extra solvent to form the octahedral arrangement. The d-d absorption energies differ between **1** and **2**, which may originate from the difference in σ-donating capability between phen and bpy. A similar difference is observed in [Cu(acac)(N^N)(ClO_4)] (N^N = phen, bpy) [21].

2.7. Thermochromism

Compounds **1** and **2** exhibited distinctive quasi-reversible thermochromism in methanol solution. The colors of the solutions gradually changed from blue via green to yellow-red on heating (Fig. S2, supplementary material). The color change rate on heating appeared to be faster than that during cooling. The change on heating is rapid, while it takes about 2 hours for the yellow-red solution to return blue despite roughly equal heating/cooling rates. In acetone and acetonitrile, however, both complexes exhibited irreversible thermochromism, exhibiting color change from blue to brick-red upon heating (Fig. S3, supplementary material). In the UV-Vis spectra for all the solutions, the change accompanied an increase of a peak at around 25000 cm^{-1}, whereas the d-d absorption peak at around 16500 cm^{-1} remained the same. This feature is similar to that found in [Cu(Cl-acac)(diamine)]ClO_4 in pyridine, except that the intensity of the d-d absorption changes as a function of temperature in this case [9]. A suggested mechanism for the thermochromism of this

complex involves ligand exchange with the solvent, to form [Cu(Cl-acac)(pyridine)$_4$]ClO_4. Based on this, we speculate that the N^N ligands in **1** and **2** are also replaced by the solvent at high temperatures, although the proper mechanism is still unknown. Solids crystals of the solvated complexes did not show thermochromism.

3. Conclusions

A series of solvated complexes derived from **1** and **2** have been prepared and structurally characterized, which enabled direct comparison of coordination structures and chromic properties of solvatochromic copper(II) complexes. It should be noted that in general, structural characterization of HMPA coordinated copper(II) complexes are rare. A variety of the d-d transition energies in solvated coordinated complexes in the solid state can be quantitatively explained in terms of the difference of the axial Cu−O bond lengths, which are further correlated with the donor number of the ligand. Understanding the relationship between the d-d transition energies and the coordination geometries of solvent-coordinated complexes would lead to the development of new and effective strategies for the construction of solvatochromic materials.

4. Experimental Section

4.1. Materials and instrumentations

All reagents and solvents were purchased from commercial suppliers and used without further purification. Infrared (IR) spectra were recorded on a Shimadzu IRAffinity-1 spectrometer as KBr pellets in the 4000–400 cm^{-1} range. Elemental analyses were performed by using a Yanagimoto C-H-N elemental analyzer (MT-5). Thermogravimetric (TG) analyses were performed under an argon atmosphere at a heating rate of 5 K min^{-1} on MAC science TG-DTA 2000S in the temperature range of 30–150 °C. The solid state UV-Vis spectra were recorded on a JASCO V-570

UV/VIS/NIR spectrophotometer, and were measured by the transmission method as KBr pellets. The solution-state UV-Vis spectra were recorded on a Shimadzu UV mini-240 spectrophotometer equipped with a temperature controller in the 700–300 nm range. DFT calculations were performed with Spartan ′10 V1.1 (Wavefunction Inc.) at the B3LYP/6-31G level.

*4.2. Preparation of [Cu(acac)(phen)]BPh_4 (**1**) and its complexes with solvent molecules*

An ethanol solution (5 mL) of $Cu(NO_3)_2 \cdot 3H_2O$ (0.24 g, 1.0 mmol) was mixed with an ethanol solution (2 mL) of 1,10-phenanthoroline (0.20 g, 1.0 mmol) and stirred for 10 min to give a blue precipitate. The precipitate was collected by filtration and washed with ethanol and diethylether. The powder was suspended in ethanol (30 mL), to which acetylacetone (0.10 mL, 1.0 mmol) and Na_2CO_3 (0.05 g, 0.5 mmol) were added and stirred for 30 min. The resulting dark blue solution was filtered to remove $NaNO_3$ and unreacted Na_2CO_3. To this filtrate was added an ethanol solution (2 mL) of $NaBPh_4$ (0.34 g, 1.0 mmol) and then a violet microcrystalline powder precipitated immediately. After stirring 10 min, the precipitate was filtered and washed with water, ethanol, and diethylether to give 0.48 g of the desired product in 73% yield. IR (KBr, cm^{-1}) 1568, 1522, 1427, 1371, 845, 734, and 611. Anal. Calcd for $C_{41}H_{35}BCuN_2O_2$ C, 74.38; H, 5.33; N, 4.23%. Found C, 74.29; H, 5.10; N, 4.26%. X-Ray quality crystals were grown by slow evaporation of a methanol solution at ambient temperature. **1**(HMPA), **1**(Py), **1**(DMSO), **1**(DMF), **1**(acetone), **1**(MeCN)·MeCN, and **1**·$MeNO_2$ were obtained by slow evaporation of corresponding solutions. IR (KBr, cm^{-1}) **1**(HMPA): 980 ν(P=O); **1**(DMSO): 1026 ν(S=O); **2**(DMF): 1666 $\nu(C=O)_{DMF}$; **1**(acetone): 1699 $\nu(C=O)_{acetone}$; **1**(MeCN)·MeCN: 2294, 2254 ν(C≡N); **1**·$MeNO_2$: 1371 ν(N−O).

*4.3. Preparation of [Cu(acac)(bpy)]BPh_4 (**2**) and its complexes with solvents*

The procedure was similar to that described for the preparation of **1**, except that 0.16 g (1.0 mmol) of 2,2′-bipyridyl was used instead of phen. Product **2** was obtained in 75% yield (0.48 g). IR (KBr, cm^{-1}) 1568, 1520, 1474, 1375, 1314, 937, and 733. Anal. Calcd for $C_{39}H_{35}BCuN_2O_2$ C,

73.41; H, 5.53; N, 4.39%. Found C, 73.18; H, 5.23; N, 4.43%. X-Ray quality crystals were grown by slow evaporation of an acetone solution. **2**(Py), **2**(DMSO), **2**(DMF)·DMF, and **2**(MeOH) were obtained by slow evaporation of corresponding solutions. IR (KBr, cm^{-1}) **2**(DMSO): 1026 ν(S=O); **2**(DMF)·DMF: 1656, 1675 $\nu(C=O)_{DMF}$; **2**(MeOH): 3518 ν(O−H).

4.4. X-ray Crystallography

X-ray diffraction data for single crystals of solvated complexes **1**(HMPA), **1**(Py), **1**(DMSO), **1**(DMF), **1**(acetone), **1**(MeCN)·MeCN, **1**·$MeNO_2$, **2**(Py), **2**(DMSO), **2**(DMF)·DMF, and **2**(MeOH) were collected on a Bruker APEX II Ultra CCD diffractometer using Mo K_α radiation (λ = 0.71073 Å) at a sample temperature of 100 K. Data for compounds **1** and **2** were collected on a Rigaku R-AXIS RAPID image plate diffractometer using Mo K_α radiation (λ = 0.71073 Å) at a sample temperature of 293 K. The structures were solved by the direct method (SIR 97 [34]) and refined on F^2 by using SHELX-97 [35]. An empirical absorption correction was applied (SADABS [36]). The non-hydrogen atoms were refined anisotropically. The hydrogen atoms attached to carbon atoms were inserted at the calculated positions and allowed to ride on their respective parent atoms. The hydroxyl hydrogen in **2**(MeOH) was located from the electron density map and refined at fixed distances from the respective parent atom.

Crystallographic parameters for the solvent-coordinated complexes derived from **1** and **2** are listed in Tables 4 and 5, respectively, and those for **1**, **2**, and **1**·$MeNO_2$ are listed in Table 6. Selected bond lengths and Cu···Cu distances (Å) are given in Tables 7 and 8.

Appendix A. Supplementary data

CCDC 838663–838672 and 867907–867909 contains the supplementary crystallographic data for **1**, **2**, **1**(DMSO), **1**(DMF), **1**(acetone), **1**(MeCN)·MeCN, **1**·$MeNO_2$, **2**(DMSO), **2**(DMF)·DMF, **2**(MeOH), **2**(Py), **1**(Py), and **1**(HMPA), respectively. These data can be obtained free of charge via http://www.ccdc.cam.ac.uk/conts/retrieving.html, or from the Cambridge Crystallographic Data

Centre, 12 Union Road, Cambridge CB2 1EZ, UK; fax: (+44) 1223-336-033; or e-mail: deposit@ccdc.cam.ac.uk.

Appendix B. Supplementary material

Photographs of single crystals, solvatochromism and thermochromism for the complexes in this context.

Acknowledgements

This work was supported by a research grant from Dean of Graduate School of Engineering at Kyoto University. The authors wish to express their thanks to Prof. T. Uemura and Dr. S. Horike (Kyoto University) for their helpful discussion. R.H. is grateful to Prof. K. Ohe, Prof. T. Tanaka, and Prof. Y. Matano (Kyoto University) for their continued encouragement.

[1] Y. Fukuda (Ed.), Inorganic Chromotropism: Basic Concepts and Applications of Colored Materials, Kodansha/Springer Tokyo, 2007.

[2] W. Linert, Y. Fukuda, A. Camard, Coord. Chem. Rev. 218 (2001) 113.

[3] U. El-Ayaan, F. Murata, Y. Fukuda, Monatsh. Chem. 132 (2001) 1279.

[4] W. Linert, Chem. Soc. Rev. (1994) 429.

[5] W. Linert, J. Chem. Inf. Comput. Sci. 32 (1992) 221.

[6] W. Linert, V. Gutmann, Coord. Chem. Rev. 117 (1992) 159.

[7] H. Golchoubian, E. Rezaee, G. Bruno, H.A. Rudbari, Inorg. Chim. Acta 366 (2011) 290.

[8] H. Golchoubian, G. Moayyedi, G. Bruno, A. Rudbari, Polyhedron 30 (2011) 1027.

[9] H. Golchoubian, E. Rezaee, J. Mol. Struc. 927 (2009) 91.

[10] H. Golchoubian, E. Rezaee, J. Mol. Struc. 929 (2009) 154.

[11] A.A.A. Abu-Hussen, W. Linert, J. Coord. Chem. 62 (2009) 1388.

[12] S. Noro, N. Yanai, S. Kitagawa, T. Akutagawa, T. Nakamura, Inorg. Chem. 47 (2008) 7360.

[13] H. Asadi, H. Golchoubian, R. Welter, J. Mol. Struc. 779 (2005) 30.

[14] H. Miyamae, H. Kubo, G. Hihara, K. Sone, Bull. Chem. Soc. Jpn. 71 (1998) 2621.

[15] J. Labuda, K. Mafune, Y. Fukuda, Bull. Chem. Soc. Jpn. 63 (1990) 2610.

[16] R.W. Soukup, R. Schmid, J. Chem. Educ. 62 (1985) 459.

[17] A.M. Madalan, N. Avarvari, M. Andruh, Cryst. Growth Des. 6 (2006) 1671.

[18] A.M. Madalan, V.Ch. Kravtsov, Y.A. Simonov, V. Voronkova, L. Korobchenko, N. Avarvari, M. Andruh, Cryst. Growth Des. 5 (2005) 45.

[19] A.M. Madalan, V.Ch. Kravtsov, D. Pajic, K. Zadro, Y.A. Simonov, N. Stanica, L. Ouahab, J. Lipkowski, M. Andruh, Inorg. Chim. Acta 357 (2004) 4151.

[20] A. Paulovicova, U. El-Ayaan, Y. Fukuda, Inorg. Chim. Acta 321 (2001) 56.

[21] C.-C. Su, S.-P. Wu, C.-Y. Wu, T.-Y. Chang, Polyhedron 14 (1995) 267.

[22] A.W. Addison, T.N. Rao, J. Reedijk, J. van Rijn, G.C. Verschoor, J. Chem. Soc., Dalton Trans. (1984) 1349.

[23] D.-M. Xie, X.-J. Ma, W.-J. Feng, Z. Shu, Z.-M. Jin, Acta Crystallogr., Sect. E. 63 (2007) m1473.

[24] T. Hosokawa, M. Takano, S. Murahashi, J. Am. Chem. Soc.118 (1996) 3990.

[25] R. Horikoshi, M. Mikuriya, Bull. Chem. Soc. Jpn. 78 (2005) 827.

[26] J.B. Lambert, Z. Liu, J. Chem. Crystallogr. 37 (2007) 629.

[27] A. Camard, Y. Ihara, F. Murata, K. Mereiter, Y. Fukuda, W. Linert, Inorg. Chim. Acta 358 (2005) 409.

[28] D. Black, A.J. Blake, R.L. Finn, L.F. Lindoy, A. Nezhadali, G. Rougnaghi, P.A. Tasker, M. Schröder, Chem. Commun. (2002) 340.

[29] M. Du, Y.-M. Guo, S.-T. Chen, X.-H. Bu, J. Ribas, Inorg. Chim. Acta 364 (2003) 207.

[30] C. Gkioni, A.K. Boudalis, Y. Sanakis, L. Leondiadis, V. Psycharis, C.P. Raptopoulou, Polyhedron 27 (2008) 2315.

[31] R.I. Butcher, W. Towns, Acta Crystallogr., Sect. E. 63 (2002) m2863.

[32] N. Okabe, Y. Muranishi, Y. Wada, Acta Crystallogr., Sect. C. 58 (2002) m511.

[33] C. Janiak, J. Chem. Soc., Dalton Trans. (2000) 3885.

[34] A. Altomare, M.C. Burla, M. Cavalli, G.L. Casvarano, C. Giacovazzo, A. Gagliardi, A.G.G. Moliterni, G. Polidori, R. Spagna, J. Appl. Cryst. 32 (1999) 115.

[35] G.M. Sheldrick, SHELX97, Programs for the solution for crystal structure, University of Göttingen, Göttingen, Germany, 1998.

[36] G.M. Sheldrick, SADABS, Program for semi-empirical absorption correction, University of Göttingen, Göttingen, Germany, 1996.

[37] V. Gutmann, Coord. Chem. Rev. 18 (1976) 225.

Figures

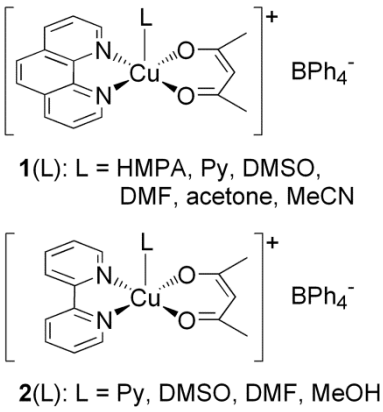

Fig. 1. Illustrations of **1**, **2** and their solvated derivatives.

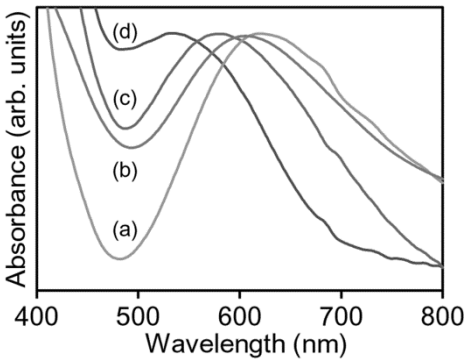

Fig. 2. Solid state UV-Vis absorption spectra of **1** and its solvent coordinated derivatives: (a) **1**(HMPA), (b) **1**(DMSO), (c) **1**(acetone) and (d) **1**.

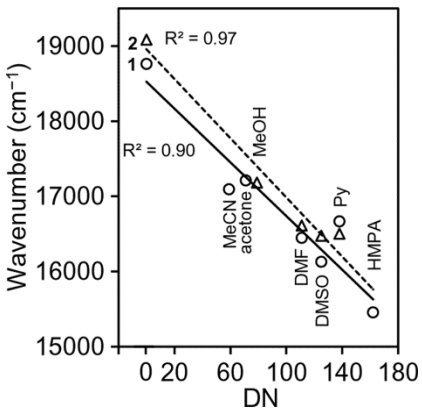

Fig. 3. Solid state d-d transition energies of the solvated complexes derived from **1** (circles) and **2** (triangles) plotted versus the donor number of the axial ligand. The solid line and dashed line

represent linear correlations for **1** and **2**, respectively.

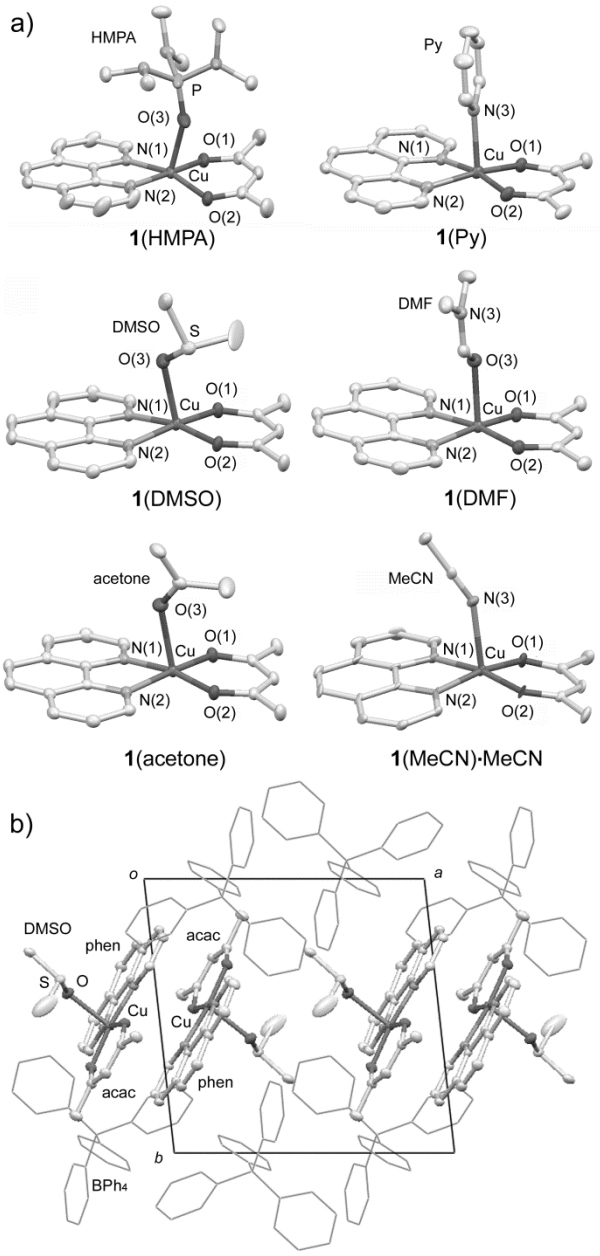

Fig. 4. a) Molecular structures of the cations in **1**(HMPA), **1**(Py), **1**(DMSO), **1**(DMF), **1**(acetone), and **1**(MeCN)·MeCN. b) Packing diagram of **1**(DMSO) viewed along the *c* axis, showing head-to-tail dimers of the cations. Hydrogen atoms are omitted for clarity. Only one of the disordered components of DMSO is shown for **1**(DMSO).

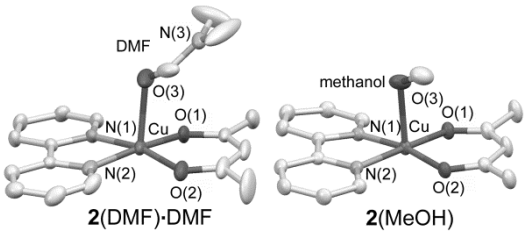

Fig. 5. Molecular structures of the cations in **2**(DMF)·DMF (left) and **2**(MeOH) (right). Hydrogen atoms are omitted for clarity.

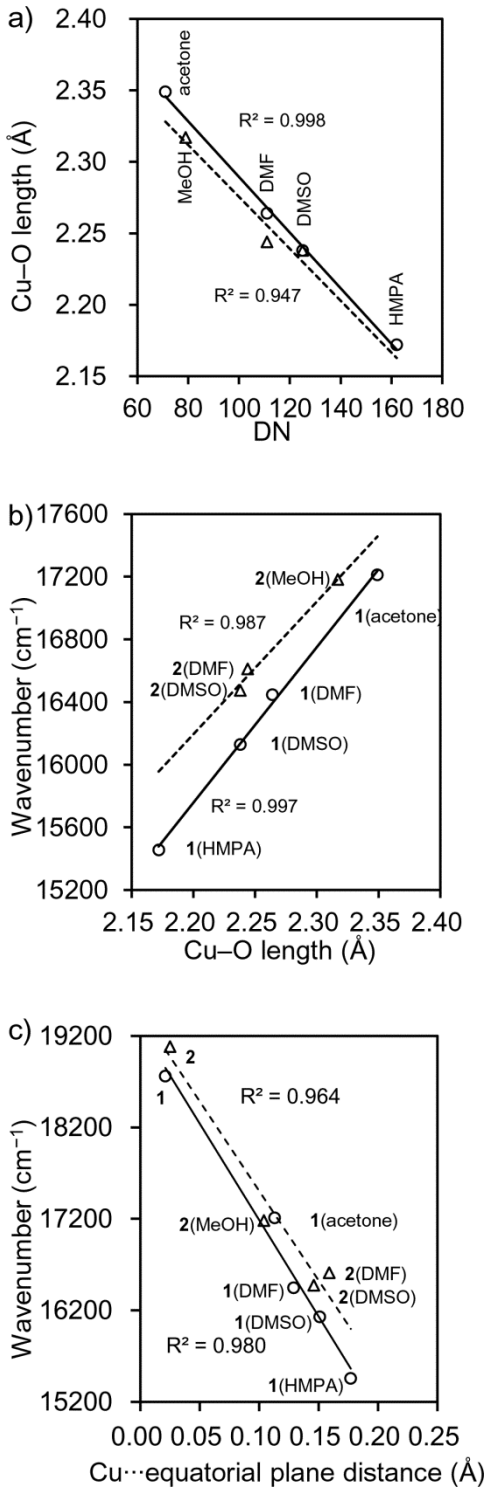

Fig. 6. a) Axial Cu−O bond lengths (Å) in solvent-coordinated complexes from **1** (circles) and **2** (triangles) plotted versus the donor number of the axial ligand. b) d-d transition energies of the solvent-coordinated complexes plotted versus the axial Cu−O bond lengths (Å). c) d-d transition energies of the solvent-coordinated complexes plotted versus the Cu···equatorial plane distances. Solid line and dashed line represent linear correlations for **1** and **2**, respectively.

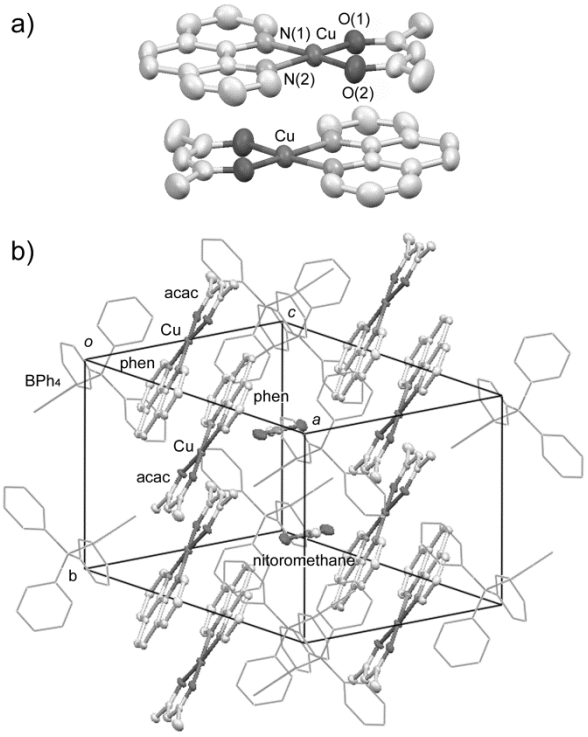

Fig. 7. a) Head-to-tail dimer structure of the cations in **1**. b) Packing diagram of **1**·$MeNO_2$. Hydrogen atoms are omitted for clarity.

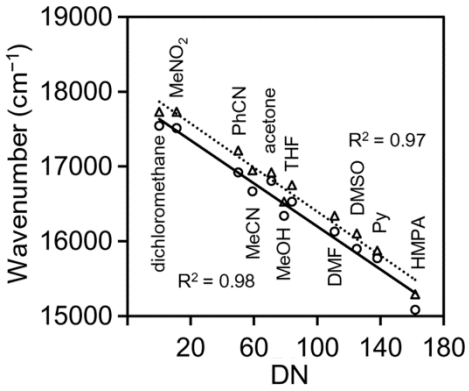

Fig. 8. d-d transition energies of the axial ligand complexes derived from **1** (circles) and **2** (triangles) in solutions plotted versus the donor number of the solvents. Solid line and dashed line represent linear correlations for **1** and **2**, respectively.

Tables

Table 1

d-d Transition energies (ν_{max}) in **1**, **2**, and their solvated complexes in the solid state.

Axial ligand	Compound	ν_{max} (cm^{-1})	Compound	ν_{max} (cm^{-1})	Donor Number [37] ($kJmol^{-1}$)
HMPA	**1**(HMPA)	15456			162
Py	**1**(Py)	16667	**2**(Py)	16502	138
DMSO	**1**(DMSO)	16129	**2**(DMSO)	16474	125
DMF	**1**(DMF)	16447	**2**(DMF)·DMF	16611	111
MeOH			**2**(MeOH)	17182	79
acetone	**1**(acetone)	17212			71
MeCN	**1**(MeCN)·MeCN	17094			59
none	**1**	18762	**2**	19084	0

Table 2

Weight loss temperatures and ratios corresponding to the loss of axial ligands from solvated complexes determined by TG analysis.

Complex	Weight loss temperature (°C)	Observed weight loss (%)	Calculated weight loss (%)	Boiling point of coordination solvent (°C)
1(HMPA)	115–*		21.3	235
1(Py)	105–*		10.7	115
2(Py)	115–*		11.0	
1(DMSO)	135–*		10.6	189
2(DMSO)	135–*		10.9	
1(DMF)	80–*		9.9	153
2(DMF)·DMF	70–*		18.6	
2(MeOH)	60−100	4.4	4.8	65
1(acetone)	80−120	8.1	8.1	56
1(MeCN)·MeCN	50−100	10.5	11.0	82

* unclear end point

Table 3

d-d Transition energies (ν_{max}) of **1** and **2** in various solvents at concentrations of 2 mM.

Solvent	ν_{max} / cm^{-1} (ε / $dm^3mol^{-1}cm^{-1}$)		Donor Number [37] ($kJmol^{-1}$)
	1	**2**	
HMPA	15083 (74)	15291 (67)	162
Py	15773 (70)	15873 (86)	138
DMSO	15898 (58)	16103 (63)	125
DMF	16129 (70)	16340 (65)	111
THF	16529 (50)	16750 (58)	84
MeOH	16340 (57)	16529 (60)	79
acetone	16807 (56)	16920 (57)	71
MeCN	16667 (60)	16949 (64)	59
PhCN	16920 (62)	17212 (62)	50
$MeNO_2$	17513 (64)	17730 (62)	11
dichloromethane	17544 (54)	17730 (57)	0

Table 4

Crystallographic parameters for solvated complexes derived from **1**

Compound	**1**(HMPA)	**1**(Py)	**1**(DMSO)	**1**(DMF)	**1**(acetone)	**1**(MeCN)·MeCN
Empirical formula	$C_{47}H_{53}BCuN_5O_3P$	$C_{46}H_{40}BCuN_3O_2$	$C_{43}H_{41}BCuN_2O_3S$	$C_{44}H_{42}BCuN_3O_3$	$C_{44}H_{41}BCuN_2O_3$	$C_{45}H_{41}BCuN_4O_2$
M / g mol^{-1}	841.26	741.16	740.19	735.16	720.14	744.17
T / K	100	100	100	100	100	100
Crystal size / mm	0.64×0.62×0.61	0.71×0.37×0.31	0.83×0.44×0.39	0.47×0.38×0.33	0.89×0.43×0.31	0.27×0.25×0.15
Space group	*C*2/c	*P*-1	*P*-1	*P*2/c	*P*-1	*P*-1
Crystal system	monoclinic	triclinic	triclinic	monoclinic	triclinic	triclinic
a / Å	22.791(3)	12.568(2)	11.800(2)	12.514(2)	11.789(2)	11.783(5)
b / Å	17.884(3)	13.539(2)	12.520(2)	22.090(3)	12.408(2)	11.896(5)
c / Å	21.249(3)	13.584(3)	13.424(2)	16.948(2)	13.424(2)	14.688(5)
α / °	90	62.347(2)	67.511(2)	90	67.822(1)	75.095(5)
β / °	95.832(2)	79.690(2)	84.052(2)	127.651(6)	84.785(2)	73.466(5)
γ / °	90	64.674(2)	81.923(2)	90	81.783(2)	88.119(5)
V / Å^3	8616(2)	1850.1(6)	1811.5(5)	3709.3(8)	1798.2(4)	1905.5(13)
Z	8	2	2	4	2	2
D_{calc} / g cm^{-3}	1.297	1.330	1.357	1.316	1.330	1.297
Absorption coefficient / mm^{-1}	0.591	0.634	0.704	0.634	0.651	0.616
Data / restraints / parameters	7599 / 0 / 582	6390 / 0 / 480	6236 / 18 / 499	6988 / 0/ 473	6212 / 0 /464	6363 / 0 / 481
Reflections collected	20371	8838	8612	9950	8597	8819
GOF on F^2	1.014	1.102	1.131	1.040	1.074	1.008
R_1,[a] wR_2 [$I > 2\sigma(I)$][b]	0.0331, 0.0880	0.0357, 0.0909	0.0341, 0.1035	0.0295, 0.0775	0.0287, 0.0746	0.0341, 0.824

[a] $R_1 = \sum||F_o|-|F_o|| / \sum|F_o|$. [b] $wR_2 = [\sum w(F^2_o-F^2_c)^2 / \sum w(F^2_o)^2]^{1/2}$.

Table 5

Crystallographic parameter for solvated complexes derived from **2**

Compound	**2**(Py)	**2**(DMSO)	**2**(DMF)·DMF	**2**(MeOH)
Empirical formula	$C_{44}H_{40}BCuN_3O_2$	$C_{41}H_{41}BCuN_2O_3S$	$C_{42}H_{42}BCuN_3O_3$	$C_{40}H_{39}BCuN_2O_3$
M / g mol^{-1}	717.14	716.17	711.14	670.08
T / K	100	100	100	100
Crystal size / mm	0.50×0.43×0.16	0.80×0.39×0.25	0.63×0.38×0.13	0.70×0.46×0.28
Space group	*P*-1	*P*-1	*P*-1	*P*-1
Crystal system	triclinic	triclinic	triclinic	triclinic
a / Å	11.241(2)	11.751(2)	9.282(5)	10.945(5)
b / Å	13.224(2)	12.695(2)	14.526(5)	11.717(5)
c / Å	13.932(2)	13.084(2)	14.961(5)	14.976(5)
α / °	66.344(2)	66.439(2)	101.665(5)	70.189(5)
β / °	72.304(2)	87.653(2)	93.767(5)	70.686(5)
γ / °	86.489(2)	82.508(2)	104.704(5)	73.282(5)
V / Å^3	1802.8(4)	1773.7(5)	1896.2(14)	1671.5(12)
Z	2	2	2	2
D_{calc} / g cm^{-3}	1.321	1.341	1.246	1.331
Absorption coefficient / mm^{-1}	0.648	0.716	0.617	0.695
Data / restraints / parameters	6243 / 0 / 462	6151 / 0 / 446	7014 / 0 / 455	5696 / 0 / 431
Reflections collected	8656	8516	9491	7660
GOF on F^2	1.058	1.046	1.055	1.032
R_1,[a] wR_2 [$I > 2\sigma(I)$][b]	0.0280, 0.0752	0.0374, 0.0945	0.0436, 0.0544	0.0378, 0.0936

[a] $R_1 = \sum||F_o|-|F_o|| / \sum|F_o|$. [b] $wR_2 = [\sum w(F^2_o-F^2_c)^2 / \sum w(F^2_o)^2]^{1/2}$.

Table 6

Crystallographic parameters for complexes without axial ligands

Compound	**1**	**2**	**1**·$MeNO_2$
Empirical formula	$C_{41}H_{35}BCuN_2O_2$	$C_{39}H_{35}BCuN_2O_2$	$C_{42}H_{38}BCuN_3O_4$
M / g mol^{-1}	662.07	638.04	723.10
T / K	296	296	100
Crystal size / mm	0.42×0.40×0.21	0.50×0.50×0.20	0.52×0.32×0.30
Space group	*P*-1	*P*-1	*P*-1
Crystal system	triclinic	triclinic	triclinic
a / Å	11.643(1)	11.812(5)	12.043(5)
b / Å	12.124(1)	11.823(5)	12.767(5)
c / Å	13.302(1)	13.095(5)	12.908(5)
α / °	90.989(2)	92.537(5)	74.112(5)
β / °	106.427(2)	107.059(5)	66.607(5)
γ / °	111.887(2)	110.862(5)	88.100(5)
V / Å^3	1655.2(2)	1610.8(11)	1745.5(12)
Z	2	2	2
D_{calc} / g cm^{-3}	1.328	1.315	1.376
Absorption coefficient / mm^{-1}	0.699	0.715	0.674
Data / restraints / parameters	7495 / 0 / 425	7249 / 0 / 406	6418 / 0 / 463
Reflections collected	16329	15616	8583
GOF on F^2	1.095	1.086	1.040
R_1,[a] wR_2 [$I > 2\sigma(I)$][b]	0.0364, 0.1042	0.0431, 0.1210	0.0458, 0.1062

[a] $R_1 = \Sigma ||F_o|-|F_o|| / \Sigma |F_o|$. [b] $wR_2 = [\Sigma w(F^2_o-F^2_c)^2 / \Sigma w(F^2_o)^2]^{1/2}$.

Table 7

Selected coordination distances and Cu···Cu distances (Å) in **1** and its solvated complexes

Compound	**1**(HMPA)	**1**(Py)	**1**(DMSO)	**1**(DMF)	**1**(acetone)	**1**(MeCN)·MeCN	**1**	**1**·$MeNO_2$
Cu–O1	1.916(1)	1.924(2)	1.916(2)	1.915(1)	1.908(1)	1.900(2)	1.886(2)	1.904(2)
Cu–O2	1.926(1)	1.911(2)	1.913(2)	1.911(1)	1.905(1)	1.914(2)	1.886(2)	1.900(2)
Cu–N1	2.014(2)	2.016(2)	2.015(2)	2.003(1)	2.007(1)	2.015(2)	1.987(2)	1.991(2)
Cu–N2	2.015(2)	2.015(2)	2.010(2)	2.022(1)	2.010(1)	2.004(2)	1.992(2)	2.002(2)
Cu–O3 (axial ligand)	2.172(2)	–	2.238(16)	2.264(1)	2.349(1)	–	–	–
Cu–N3 (axial ligand)	–	2.268(2)	–	–	–	2.408(2)	–	–
Cu···equatorial plane*	0.177	0.172	0.151	0.129	0.113	0.163	0.021	0.044
Cu···Cu	6.365	4.134	4.902	3.815	4.853	6.155	3.562	5.732

* least square O1–O2–N1–N2 plane

Table 8

Selected coordination distances and Cu···Cu distances (Å) in **2** and its solvated complexes

Compound	**2**(Py)	**2**(DMSO)	**2**(DMF)·DMF	**2**(MeOH)	**2**
Cu–O1	1.933(1)	1.915(2)	1.922(2)	1.913(2)	1.890(2)
Cu–O2	1.926 (1)	1.916(2)	1.912((2)	1.907(2)	1.892(2)
Cu–N1	2.000(1)	2.000(2)	1.988(2)	1.989(2)	1.977(2)
Cu–N2	2.009(1)	1.995(2)	1.999(2)	1.998(2)	1.970(2)
Cu–O3 (axial ligand)	–	2.238(2)	2.244(2)	2.317(2)	–
Cu–N3 (axial ligand)	2.295(1)	–	–	–	–
Cu···equatorial plane*	0.192	0.146	0.159	0.104	0.025
Cu···Cu	4.588	4.192	4.796	3.656	3.570

* least square O1–O2–N1–N2 plane

Appendix B. Supplementary material

Copper(II) solvatochromic complexes [Cu(acac)(N^N)(ligand)]BPh_4 with various axial ligands. Correlation between coordination geometries and d-d transition energies (acac = acetylacetonato, N^N = 1,10-phenanthoroline, 2,2′-bipyridyl)

Ryo Horikoshi [a,*], Yusuke Funasako [b], Takeshi Yajima [a], Tomoyuki Mochida [b], Yoji Kobayashi [a], Hiroshi Kageyama [a]

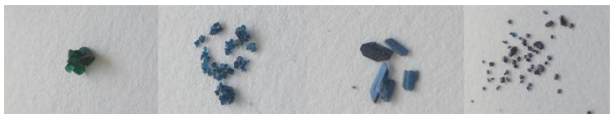

a b c d

Fig. S1. Photographs of single crystals of a) **1**(HMPA), b) **1**(DMF), c) **1**(acetone), and d) **1**.

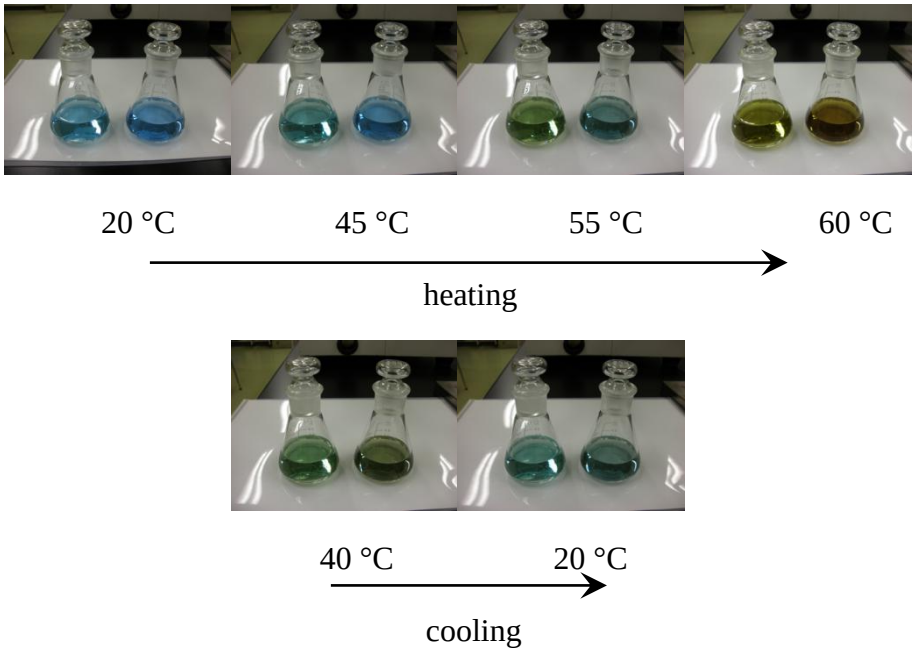

Fig. S2. Thermochromism of **1** (right) and **2** (left) in MeOH solutions.

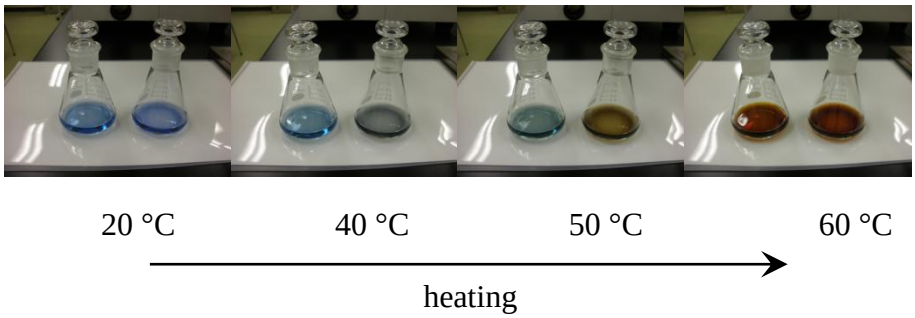

Fig. S3. Thermochromism of **1** (right) and **2** (left) in acetone solutions.